

Star formation and environment in clusters up to $z \sim 2.2$

A. Raichoor and S. Andreon

INAF – Osservatorio Astronomico di Brera, via Brera 28, 20121 Milan, Italy
e-mail: [anand.raichoor; stefano.andreon]@brera.inaf.it

Received 1 September 2011 / Accepted 24 October 2011

ABSTRACT

Context. The dependence of galaxy star-formation activity on environment – especially in clusters – at high redshift is still poorly understood, as illustrated by the still limited number of $z \gtrsim 1.4$ clusters on the one hand, and by the still debated star formation-density relation at high redshift on the other hand.

Aims. The $z_{\text{phot}} \sim 2.2$ JKCS 041 cluster allows us to probe this environmental dependence of star formation activity at an unprecedented combination of redshifts and environments. Its study permits us to enhance our knowledge of high redshift clusters and to put strong leverage on observational constraints of galaxy evolution models.

Methods. We analyze deep $u^*g'r'i'z'JHK_s$ images from the CFHTLS/WIRDS surveys, which cover the JKCS 041 cluster field. We first estimate photometric redshifts based on multi-wavelength photometry. We then lead a careful analysis to test the presence of a Butcher-Oemler effect. We work on galaxies within $2 \times r_{200}$ with masses $M \geq 1.34 \times 10^{11} M_{\odot}$, and use two comparison clusters at $z = 0$ and $z = 1$ of similar mass. We estimate the radial profiles of the fraction of blue galaxies, taking into account the star aging with decreasing redshift.

Results. After confirming the high redshift nature of JKCS 041, we find no evidence of a Butcher-Oemler effect between $z \sim 2.2$ and $z \sim 0$ for galaxies more massive than $1.34 \times 10^{11} M_{\odot}$. In the cluster center, a change greater than $\Delta f_{\text{blue}}/\Delta z = 0.16$ between $z \sim 0$ and $z \sim 2.2$ would be easily detected. We also find that JKCS 041 shows a consistent and systematic increase in the fraction of star-forming galaxies with cluster-centric distance, hence with decreasing density, for both a $M \geq 1.34 \times 10^{11} M_{\odot}$ selected sample and a lower mass sample. In particular, very few (less than 15%) star-forming galaxies are found within $r_{200}/2$ among high mass ($M \geq 1.34 \times 10^{11} M_{\odot}$) galaxies.

Conclusions. Our results show that the present-day star formation-density relation is already in place at $z \sim 2.2$.

Key words. galaxies: clusters: general – galaxies: evolution – galaxies: clusters: individual: JKCS 041

1. Introduction

It is known that, in the local Universe, star formation activity is correlated with galaxy environments: galaxies with low star formation rates are preferentially found in dense environment, galaxies in cluster cores being virtually all quiescent (e.g. Oemler 1974; Hogg et al. 2003; Kauffmann et al. 2004). However the various processes that led to this situation in the local Universe are still not fully understood (e.g. Treu et al. 2003). To put constraints on how this star formation-density relation, which is well-established in the local Universe, has been built through cosmic ages, one should observe galaxies at increasing look-back times and study their star formation activity with respect to the environment at fixed stellar mass, so as to isolate the role of environment. In this context, galaxy clusters provide important information, as they are the densest environments in the Universe.

It has been shown that the star formation-density relation holds out to $z \lesssim 0.8$ (e.g. Patel et al. 2011). At $z \sim 0.8-1$, while studies in low-density environments (e.g. Elbaz et al. 2007; Cooper et al. 2008) observe a reversal of the star formation-density relation, other studies focusing on cluster environments (e.g. Patel et al. 2009; Koyama et al. 2010) find that cluster core regions are devoid of star-forming galaxies. Sobral et al. (2011), studying a very wide range of environments, nicely reconcile those observations: star formation activity increases with increasing density up to $\Sigma \sim 10-30 \text{ Mpc}^{-2}$, and then decreases with increasing density for $\Sigma \gtrsim 30 \text{ Mpc}^{-2}$.

Studying a superstructure at $z \sim 1.2$, Tanaka et al. (2009) find that the star formation-density relation is already in place. When going to higher redshifts ($z \sim 1.4-1.6$), the situation is less clear. On the one hand, Hayashi et al. (2010) and Hilton et al. (2010) study the XMMXCS J2215.9-1738 cluster at $z = 1.46$ ($kT \sim 4.1 \text{ keV}$, Stanford et al. 2006; Hilton et al. 2010): looking at the [OII] and $24 \mu\text{m}$ emission respectively, both works observe a high star-formation activity at its centre. On the other hand, studies on the massive XMMU J2235-2557 cluster at $z = 1.39$ ($kT \sim 8.6 \text{ keV}$, Jee et al. 2009; Rosati et al. 2009) observe that its core region does not display any star formation activity (Lidman et al. 2008; Rosati et al. 2009; Strazzullo et al. 2010; Bauer et al. 2011). Chuter et al. (2011) and Quadri et al. (2012) study a large sample of galaxies and environments in the UKIDSS Ultra-Deep Survey (UDS, Lawrence et al. 2007; Almaini, in prep.) and find that the star formation-density relation holds out to $z \sim 1.5-1.8$. Quadri et al. (2012) also investigate the ClG J0218.3-05101 cluster at $z = 1.62$ ($kT \sim 1.7 \text{ keV}$, Papovich et al. 2010; Tanaka et al. 2010) and observe that its central region has an elevated fraction of quiescent objects relative to the field, in apparent disagreement with Tran et al. (2010), who observe an increase in the star formation activity along with the density.

Although the two clusters XMMU J2235-2557 and XMMXCS J2215.9-1738 lie at a similar redshift of $z \sim 1.4$, XMMU J2235-2557 is massive and has a well-defined red sequence down to faint galaxies, thus is likely in a very advanced evolutionary stage, whereas XMMXCS J2215.9-1738 is less massive and displays a deficit of faint galaxies on the red

sequence, thus is in a less evolved dynamical state. At lower redshift ($z \sim 0.3$), [Braglia et al. \(2009\)](#) studied the star formation activity in two clusters with opposite dynamical states: even if low star formation activity is found in both cluster cores, star formation activity is found in the less evolved cluster, out to its virial radius and beyond, while no star formation activity is found in the more evolved cluster, thus suggesting that there is a link between the dynamical state and the star formation activity in clusters. The different dynamical status may explain the conflicting evidence observed at high redshift.

The evolution of star formation activity within clusters has been studied in many papers (e.g. [Haines et al. 2009](#), and references therein), starting with the pioneering work of [Butcher & Oemler \(1984\)](#). The latter authors looked at the fraction of blue galaxies, f_{blue} , in clusters and its evolution with redshift, thus probing the impact of dense environments on star formation activity. This seminal study found an increase in f_{blue} within clusters with increasing redshifts – the so-called Butcher-Oemler effect – out to $z \sim 0.5$, thus pointing to an accelerated evolution in clusters. However, it has been subsequently shown that Butcher-Oemler effect studies may be severely affected by methodological biases. [Andreon & Etori \(1999\)](#) showed that a strong bias in the original [Butcher & Oemler \(1984\)](#) cluster sample may account for the observed effect. According to subsequent works ([De Propriis et al. 2004](#); [Goto 2005](#)), f_{blue} does not appear to depend on the cluster mass. [De Propriis et al. \(2003\)](#) illustrated that it is necessary to use a mass-selected galaxy sample: if one instead uses an optical luminosity-selected galaxy sample as [Butcher & Oemler \(1984\)](#) did, higher redshift samples will be biased towards low-mass starburst galaxies, not included in lower redshift samples, leading to an artificial increase in f_{blue} . Finally, [Andreon et al. \(2006\)](#) showed that the criterion used to define a blue galaxy needs to take into account the younger mean age of the Universe and the secular increase in the star formation rate with redshift.

Recent studies taking into account those methodological biases find no evidence of a Butcher-Oemler effect out to $z \sim 0.5$ ([Andreon et al. 2006](#); [Haines et al. 2009](#)). Nevertheless, [Andreon et al. \(2008b\)](#) did find evidence of a Butcher-Oemler effect when comparing a $z \sim 1$ cluster with local clusters.

In this paper, we take advantage of CFHTLS/WIRDS public deep images covering the $z \sim 2.2$ JKCS 041 cluster ([Andreon et al. 2009](#)) to address the aforementioned issues. The cluster JKCS 041 presents a well-defined red sequence ([Andreon & Huertas-Company 2011](#)) populated by a homogenous population of galaxies with extremely synchronized stellar ages ([Andreon 2011](#)) and extended X-ray emission with a temperature of $T = 7.3^{+6.7}_{-2.6}$ keV ([Andreon et al. 2009, 2011](#)), attesting the presence of a formed potential well, that is deep enough to heat gas to such high temperatures and retain the intracluster medium. Thus, JKCS 041 offers a unique opportunity to probe star formation activity in clusters and the Butcher-Oemler effect out to $z \sim 2.2$.

The plan of this paper is as follows: we describe in Sect. 2 the data used for JKCS 041, along with the analysis led on them. In Sect. 3, we outline how we estimated the JKCS 041 photometric redshift. We then study the Butcher-Oemler effect in Sect. 4 and the star formation activity of JKCS 041 in Sect. 5. We summarise and discuss our results in Sect. 6.

In this paper, we adopt $H_0 = 70 \text{ km s}^{-1} \text{ Mpc}^{-1}$, $\Omega_m = 0.30$, and $\Omega_\Lambda = 0.70$. All magnitudes are in the AB system and masses are computed with a [Chabrier \(2003\)](#) initial mass function (IMF). The JKCS 041 virial radius, estimated from the X-ray temperature, is $r_{200} = 1.53'$

([Andreon et al. 2009](#), $\sim 0.76 \text{ Mpc}$ at $z \sim 2.2$) and the cluster center is defined as the barycenter of the X-ray emission.

2. Data and analysis

We describe in this Section the data used for JKCS 041, along with the analysis led on them.

2.1. Data

The cluster JKCS 041 is in the $\sim 0.6 \text{ deg}^2$ area covered by the CFHTLS deep survey ($u^*g'r'i'z'$ bands) and by the WIRDS follow-up survey in the infrared filters (JHK_s bands, 50% point source completeness: $K_s = 24.7$) ([Bielby et al. 2011](#), catalogues are available at the CFHT Science Data Archive site¹). Throughout this work, we use the T0002 release of catalogues generated using the K_s -band image as a detection image and the other bands in the analysis mode. More specifically, we use magnitudes measured in $2''$ apertures ($2''$ are $\sim 17 \text{ kpc}$ at $z \sim 2.2$) for colours, and “total” magnitudes, both corrected for Galactic extinction using [Schlegel et al. \(1998\)](#).

To use these catalogues for the study of JKCS 041, we need to: a) identify stars; b) correct the underestimate of photometric errors listed in the original catalogue; c) correct for a (minor) residual photometric offset; d) measure photometric redshifts and e) correct for their systematic biases. We detail each of them in turn.

The VIMOS VLT Deep Survey project (VVDS, [Le Fèvre et al. 2005](#)) gives spectroscopic redshifts, z_{spec} , of several thousands of objects in the same area. For our spectroscopic sample, we use objects in common with the T0002 catalogues – rejecting the edgings – with $K_s \leq 23$ (see hereafter) and a secured z_{spec} (flag = 3, 4), thus yielding a spectroscopic sample of 2537 galaxies ($z_{\text{spec}} \lesssim 1.5$) and 366 stars ($z_{\text{spec}} = 0$).

2.2. Star removal

Stars are identified, and removed, in the colour-colour plane, as described in [Cowie et al. \(1994\)](#) and later studies. In the $z' - K_s$ versus (vs.) $g' - z'$ colour-colour diagram, spectroscopically-identified stars populate a narrow locus offset from galaxies, as shown in Fig. 1. We therefore classify as stars every object bluer in $z' - K_s$ than the broken line shown in Fig. 1. This criterion enables us to exclude more than 95% of the spectroscopically confirmed stars. We check that the VVDS spectroscopic star sample is unbiased (for our purposes), because it covers the same colour-colour locii as the large and representative sample in [Finlator et al. \(2000\)](#). Stars not identified as such in this phase are removed at a later stage (during the photometric redshift selection and the background statistical subtraction phase).

2.3. Photometric error correction

Owing to a slight noise correlation introduced by image resampling during the stacking, the flux errors derived by SExtractor ([Bertin & Arnouts 1996](#)) are underestimated (e.g. [Casertano et al. 2000](#); [Andreon 2001](#)). Following [Andreon \(2001\)](#), by binning the images we are able to recover the actual background noise, and thus compute the underestimation factor, thanks to the correlation being present only on small spatial scales. We

¹ <http://www1.cadc-ccda.hia-ihp.nrc-cnrc.gc.ca/cfht/WIRDST0002.html>

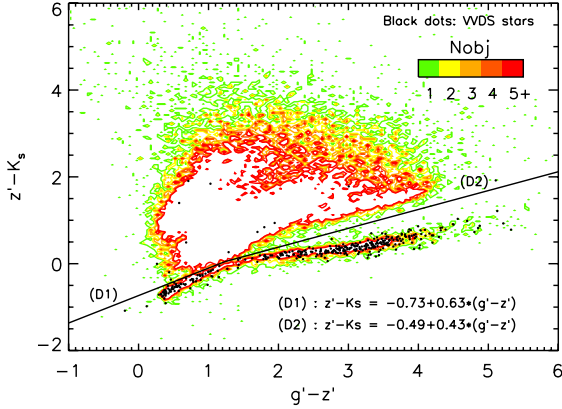


Fig. 1. Star/galaxy separation: $g' - z'$ vs. $z' - K_s$ diagram. Noisy contours give the density of objects at each location. Spectroscopically confirmed stars are marked with black dots. The broken line marks the star/galaxy separation threshold.

Table 1. Systematic offsets $m_{\text{fit}} - m_{\text{meas}}$ between measured and best-fit model magnitudes.

u^*	g'	r'	i'	z'	J	H	K_s
-0.08	0.06	0.01	0.03	-0.01	-0.05	-0.02	0.01

find a factor of 1.5 for optical bands, in agreement with Ilbert et al. (2006) and Coupon et al. (2009), and a factor of 2.0 for near-infrared bands. The larger factor for near-infrared bands is due to the native larger pixel size of the images and thus finer resampling during the stacking. After a correction for the aforementioned error underestimate, the completeness, defined as $S/N = 5$, occurs at $K_s = 23$ mag, $J = 23.6$ mag, and $z' - J = 29.5 - 1.25 \times K_s$ mag. Lower S/N data are never used in our study here and even more restrictive cuts are used in most instances, as detailed below.

2.4. Photometric redshift estimation

For photometric redshift estimation, we use EAZY (Brammer et al. 2008) with default settings and a K_s -band magnitude prior. We use both the full photometric redshift probability distribution function, $p(z)$, and z_{mp} , where the latter is a point estimate of the photometric redshift, given by the redshift posterior mean (see Sect. 2.5 of Brammer et al. 2008). As noted in previous works (e.g., Brodwin et al. 2006; Ilbert et al. 2006; Coupon et al. 2009; Ilbert et al. 2009; Barro et al. 2011), offsets in the photometric calibration or the inadequacy of the templates to reproduce all the observed spectral energy distributions (SEDs) can lead to systematic offsets in the photometric redshift estimation. The code EAZY addresses the latter by using a template error function. To fix photometric offsets, we use the subsample of our VVDS galaxies that have a S/N greater than ten in all the eight photometric bands (2013 galaxies) and we compute the mean difference between the predicted (best-fit model) and observed magnitude. More precisely, we compute this average one filter at a time, apply the photometric offsets, and iterate until the procedure converged. Five iterations are sufficient for convergence and the found offsets are listed in Table 1. These small shifts, comparable with previous works (Ilbert et al. 2006, 2009; Coupon et al. 2009; Barro et al. 2011), are applied only to the photometric redshift estimates.

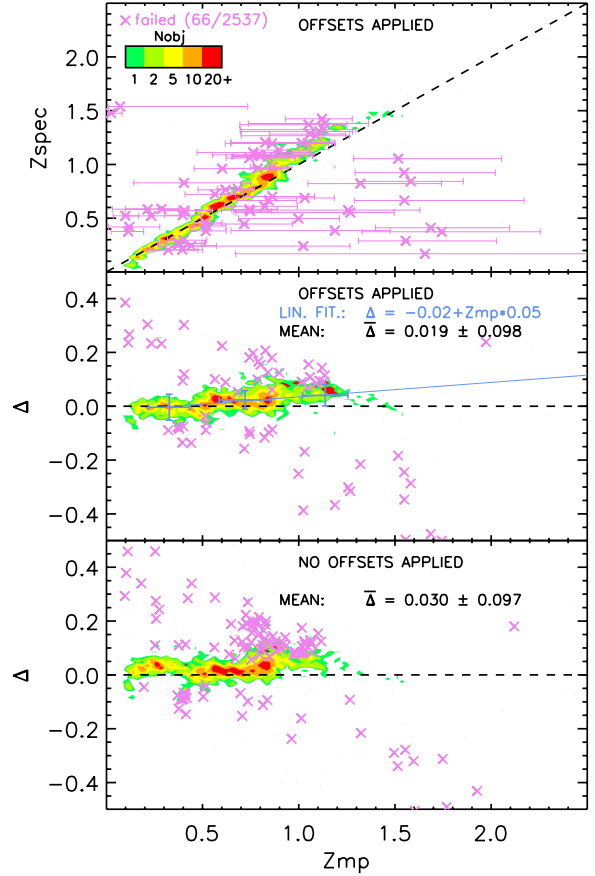


Fig. 2. Performance of the photometric redshift estimate: contours indicate the density of objects at each location. In this figure only, we consider that the photometric redshift estimate fails when z_{spec} does not belong to the 3σ confidence interval of z_{mp} (light magenta). *Upper panel:* z_{spec} vs. z_{mp} when offsets are applied. *Middle panel:* residuals $\Delta = (z_{\text{spec}} - z_{\text{mp}})/(1 + z_{\text{mp}})$ vs. z_{mp} when offsets are applied. The light blue line is a linear fit to the three points in light blue, representing the median values when the data are binned in three bins. We observe that $z_{\text{spec}} \geq 1$ galaxies tend to have their z_{mp} value underestimated (cf. light blue line). *Lower panel:* residuals Δ vs. z_{mp} when no offsets are applied.

Figure 2 shows z_{mp} vs. z_{spec} (top panel) after correction of the photometric offsets. The scatter is 0.019 ± 0.098 , much better than if the correction is not applied (0.030 ± 0.097), largely because an improvement at low redshift, as shown from comparison of residuals before and after correction (see middle and bottom panels).

Even after the correction of the photometric offsets, the photometric redshift tends to underestimate the spectroscopic redshift at $z > 1$ (see middle panel), as already noted by Brammer et al. (2008). The linear fit to the binned data (light blue) illustrates this trend. We checked that a similar underestimate of the redshift holds for the sub-sample of red galaxies, defined as $(U - V)_{\text{rest-frame}}^{\text{model}} > 1.3$ mag. We apply this last correction in the only place of this work where it is needed, that described in Sect. 3.

2.5. Background removal

When estimating the properties of the JKCS 041 galaxy population – in Sects. 4 and 5, we need to account for galaxies along the cluster line of sight, which we generally call background, by applying a two-step procedure: first, we perform a photometric

redshift selection by removing galaxies (and quasi-stellar objects) that are at $z < 1.7$ or $z > 3.5$ at $\geq 99\%$ confidence. This selection is accomplished by keeping objects with

$$\int_0^{1.7} p(z)dz \leq 0.99 \quad \text{and} \quad \int_{3.5}^{+\infty} p(z)dz \leq 0.99. \quad (1)$$

We note that the second equation removes very few objects. We note that this selection is very effective in removing “low redshift” galaxies, as it removes 2495 of the 2522 galaxies with $z_{\text{spec}} \leq 1.5$ in our VVDS sample. As later detailed, we explore other possible choices, and results are insensitive to the precise recipe adopted.

As a second stage of the background subtraction, we use a large control area ($\sim 0.1 \text{ deg}^2$ around the cluster, excluding a disk of $7'$ radius centered on the cluster) to estimate the residual background. This step also subtracts any star that has not been identified as such based on its colours.

We here analyze the impact on our sample selection of incorrect photometric redshift estimates. In Fig. 2, a sizable number of points scatters from the diagonal in the top panel. In this figure only, we consider the photometric redshift estimate to fail when z_{spec} does not belong to the 3σ confidence interval of z_{mp} (galaxies in light magenta). A large majority of the outliers are objects with fairly large errors. Most of the outliers are in the lower-right corner of the z_{spec} vs. z_{mp} plot (i.e. galaxies with overestimated photometric redshift). These galaxies increase the noisiness of our measurements but do not introduce any bias, because they remain in the sample. The most problematic data points are those of high-redshift galaxies with a largely underestimated redshift (i.e. the objects in the very top-left corner) and a nominal small redshift uncertainty. These galaxies, if they exist, would indeed be a source of incompleteness in our sample, which discards all galaxies which are at $z < 1.7$ at 99% confidence. For our spectroscopic sample, this situation never occurs; there are only two galaxies – lying at a redshift ($z_{\text{spec}} \sim 1.6$) lower than the one we are interested in – that are in a qualitatively similar situation.

3. JKCS 041 photometric redshift estimate

To estimate the JKCS 041 redshift, we select bright ($K_s \leq 21.2$) objects within a radial distance of $0.5 \times r_{200}$ and within 3σ of the $z' - J$ vs. K_s colour-magnitude relation ($1.74 \leq z' - J \leq 2.2$, Andreon 2011), because this choice maximizes the cluster membership likelihood (such bright and red galaxies are rare in the field, as measured all around the cluster). We emphasize that we do not use any photometric redshift selection in this section. For each of these eight galaxies, Fig. 3 shows their SED along with their EAZY best-fit template and, as insets, its position in the colour-magnitude diagram (*upper-left inset*) and the photometric redshift probability distribution function $p(z)$ (*lower-right inset*). We observe that the fits are of good quality and that these eight galaxies display a prominent 4000 \AA break near the J band, which a characteristic of old high-redshift galaxies. We note that the two bluest galaxies have a $p(z)$ distribution that is less peaked and slightly shifted towards lower redshifts.

In Fig. 4, we gather the photometric redshift probability distribution functions $p(z)$ for the eight selected galaxies (thin coloured lines). All the eight of these $p(z)$ distributions peak between $z \sim 1.8$ and $z \sim 2.2$. If we assume that all these eight objects belong to the cluster, the cluster photometric redshift is obtained by multiplying the $p(z)$ functions, as they have been derived from independent data. The result is plotted in Fig. 4 as a thick black line: it has a very peaked shape around $z \sim 2.0$

(1σ confidence interval: [1.97, 2.02]) in broad agreement with the photometric redshift of $z_{\text{phot}} = 2.20 \pm 0.11$ that was robustly estimated in Andreon & Huertas-Company (2011). We stress that our photometric redshift estimate is derived using a photometric redshift correction extrapolated from $z \lesssim 1.5$: it is hence slightly less robust than the Andreon & Huertas-Company (2011) estimate, which uses the red sequence and as a calibration the cluster CIG J0218.3-0510, which has a spectroscopic redshift $z_{\text{spec}} = 1.62$ (Papovich et al. 2010; Tanaka et al. 2010).

The top axis of Fig. 4 shows that JKCS 041 would have a high redshift ($z_{\text{raw}} \sim 1.8$) even when neglecting the correction for the underestimate of photometric redshift shown in Fig. 2. This underestimate suggests that there is a calibration problem with the models. Nevertheless, as model predictions match JKCS 041 colours for a redshift $z \sim 1.8$, we use in the rest of this article this value to redshift our models. This approach allows us to use predicted colours in agreement with our observations (in particular, see Fig. 9 where the predicted colours for a simple stellar population (SSP) match the red sequence).

4. Butcher-Oemler effect

The measurement of the Butcher-Oemler effect requires particular attention to the way in which the galaxies are selected in terms of mass and classified as blue/red (see Sect. 1). First, we use a mass-selected sample. We select all galaxies more massive than $1.34 \times 10^{11} M_{\odot}$, which corresponds to our completeness ($S/N = 5$) limit in the worst case (old red galaxies). For our values of mass we refer, as in previous works, to the Bruzual & Charlot (2003) model (2007 version, CB07 hereafter) mass, and specifically the mass of the gas that will eventually be turned into stars (see e.g. Longhetti & Saracco 2009, for other possible definitions of model mass). These (model) masses are computed for solar metallicity, a formation redshift of $z_f = 5$, and either SSP or an exponentially declining star-forming τ model with $0 < \text{SFH } \tau \text{ (Gyr)} \leq 10$.

4.1. Blue/red definition

We define a galaxy as blue if it is bluer than a CB07 model with $\tau = 3.7 \text{ Gyr}$, as in Andreon et al. (2004, 2006, 2008b) and Loh et al. (2008). This galaxy will be bluer by 0.2 mag in $B - V$ than red-sequence galaxies at the present epoch (which would be a blue galaxy by the original definition of Butcher & Oemler 1984). The rationale behind this choice is described in detail in Andreon et al. (2006) and Andreon (2006), but in short we take into account the stellar evolution of galaxies with time.

We emphasize that for a galaxy to be classified as blue it should be very blue, at least 0.8 mag bluer in $J - K_s$ than the red sequence. This is imposed by the requirement that we follow galaxies back in time, with a criterion independent of the redshift (under the assumption of exponentially declining star formation history). A significantly narrower selection is precluded because, at lower redshift, it would end up at the top of the red sequence.

Figure 5 shows the $J - K_s$ vs. K_s (about rest-frame $u^* - r'$ vs. r') colour-magnitude diagram for galaxies within $2 \times r_{200}$ of the cluster center and more massive than $1.34 \times 10^{11} M_{\odot}$. We adopted this colour index because it is the one that most closely matches the colour index used in our comparison sample below. As later detailed, our results do not depend on the colour index adopted. Not many galaxies are blue (below the dashed line in Fig. 5), even before accounting for any residual (after photometric redshift selection) background along the JKCS 041 line of

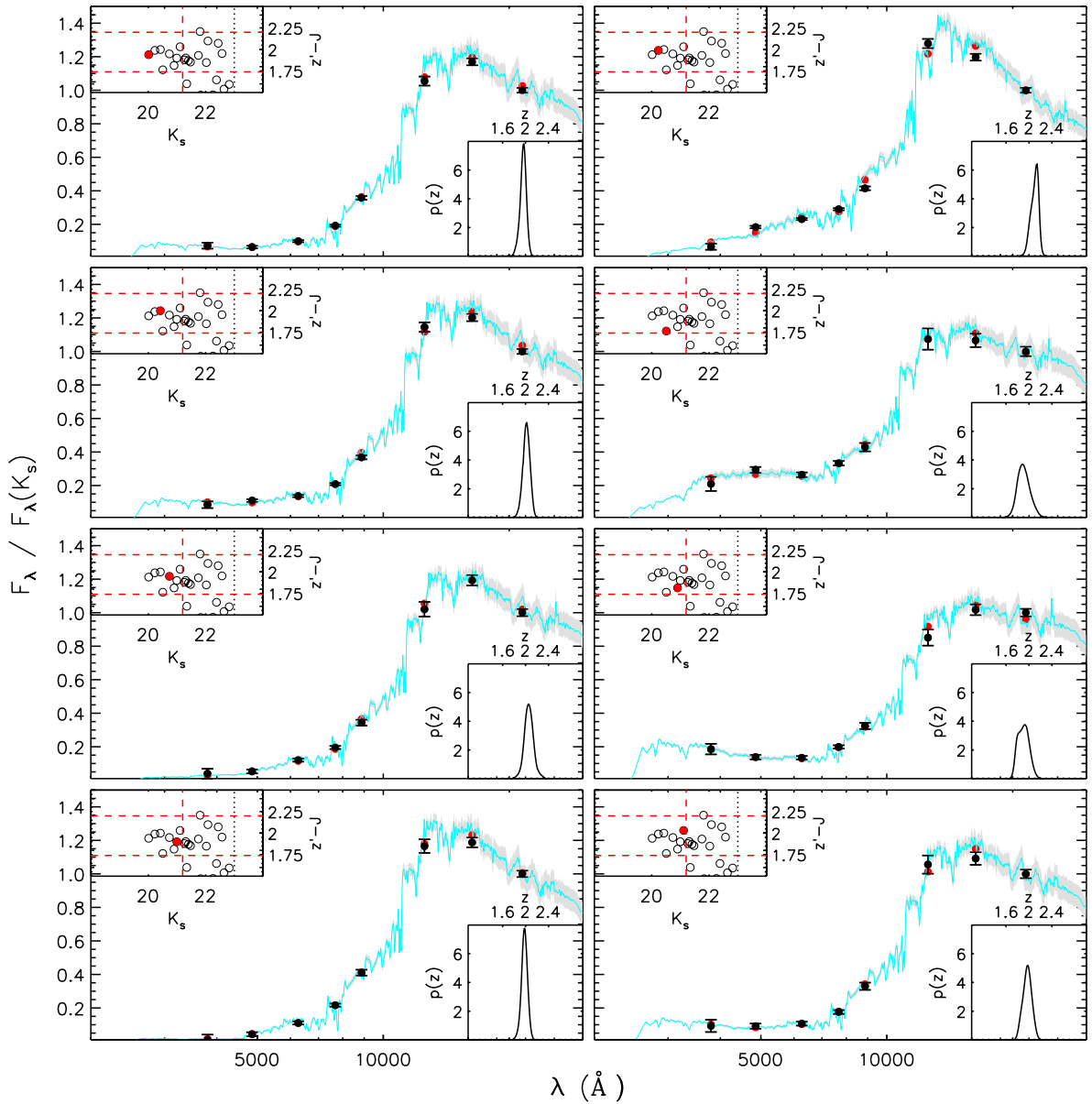


Fig. 3. JKCS 041 bright red sequence galaxies analysis. Large panels shows the normalized SED (black dots with error bars), along with the EAZY best-fit template (cyan line) and the best-fit model photometric points (red dots). The thin light gray shaded area around the best-fit template shows the model uncertainty in the best-fit template, as given in EAZY. *Upper-left insets:* colour–magnitude relation of all galaxies within $0.5 \times r_{200}$. The closed (red) point emphasizes the object whose SED is shown. Red dashed lines represent cuts in magnitude and colour used in this plot, whereas the black vertical dotted line represents the $K_s = 23$ limit. *Lower-right insets:* photometric redshift probability distribution function $p(z)$ for the considered galaxy. All those red and bright galaxies have a SED with a prominent 4000 \AA break and are well fitted with a template at $z \sim 2.0$.

sight. In addition, we underline that all (resp. more than 90%) of our sample galaxies have a $S/N \geq 10$ in K_s (resp. $J - K_s$).

4.2. Measurement of a Butcher-Oemler effect

We compute the blue fraction and the number of red and blue members galaxies accounting for residual background galaxies (i.e. along the line of sight, and not belonging to the cluster) using our control field following the Bayesian methods introduced in Andreon et al. (2006). We adopt uniform priors for the parameters. We consider three regions annuli at distinct cluster-centric radii, defined by $r/r_{200} \leq 0.5$, $0.5 < r/r_{200} \leq 1$, and $1 < r/r_{200} \leq 2$.

To provide lower redshift reference clusters, we consider RZCS 052 at $z = 1.016$ (Andreon et al. 2008b), and Abell 496 (A496 hereafter, Abell 1958) at $z = 0.033$ (Struble & Rood 1999), which were used in the Butcher-Oemler study of Andreon et al. (2008b), considering a lower mass threshold. Table 2 lists some of the key characteristics of our cluster sample used to study the Butcher-Oemler effect. As one can see, our three clusters have roughly similar masses; moreover our study shows that they also have similar richnesses (see hereafter, Fig. 6). We use as a colour index $u^* - r$ for A496 and $I - z'$ for RZCS 052, thus adopting in both cases a rest-frame u^* -like band as blue band, as for JKCS 041. We recompute the blue fraction of the A496 and RZCS 052 clusters for galaxies with $M \geq 1.34 \times 10^{11} M_\odot$.

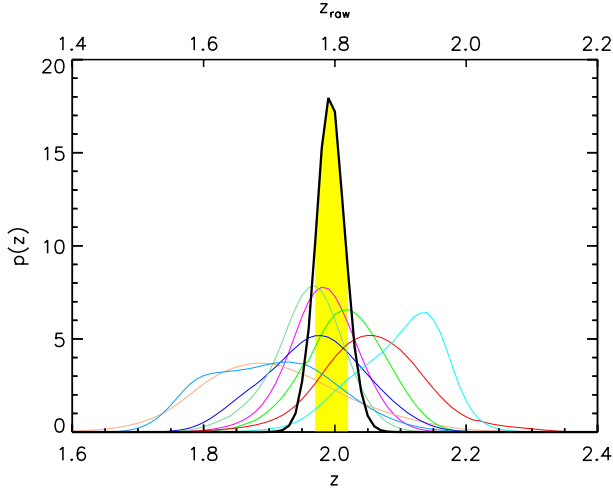


Fig. 4. JKCS 041 photometric redshift estimate: the thick black line shows the cluster photometric redshift, the thin coloured lines represent the photometric redshifts of the eight bright galaxies on the cluster red sequence shown in Fig. 3. The area shaded in yellow represents the 1σ confidence interval. The top axis shows the raw photometric redshift, which is not corrected for the known underestimate of the photometric redshifts.

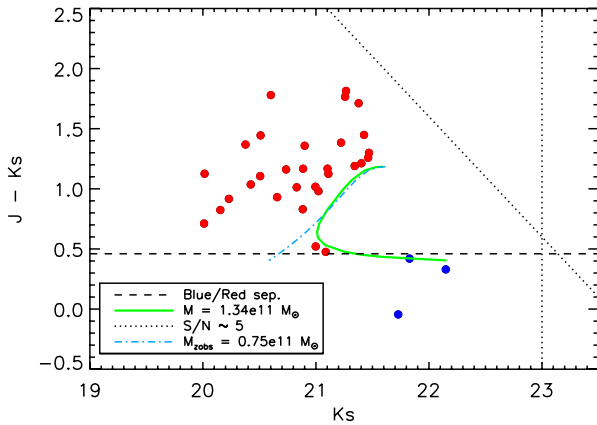


Fig. 5. Colour–magnitude diagram for galaxies along JKCS 041 line of sight (i.e. JKCS 041 and residual background galaxies) within $2 \times r_{200}$. The black dotted lines represent the $S/N \sim 5$ completeness. The green thick solid line represents the mass cut ($M = 1.34 \times 10^{11} M_{\odot}$). The dashed line indicates the blue/red threshold. For illustrative purposes, the light blue dash-dotted line represents the locus of galaxies with a mass in stars at the redshift of JKCS 041 of $M_{z_{\text{obs}}} = 0.75 \times 10^{11} M_{\odot}$.

Table 2. Cluster sample used to estimate the Butcher-Oemler effect.

Cluster	r_{200} (Mpc)	σ_v (km s^{-1})	M_{200} ($10^{14} M_{\odot}$)
A496 ^a	1.85	721^{+35}_{-30}	7.5
RzCS 052 ^b	1.04	710^{+150}_{-150}	4.0
JKCS 041 ^c	0.76	–	$4.0^{+5.3}_{-3.3}$

Notes. ^(a) Rines et al. (2005); ^(b) Andreon et al. (2008a); ^(c) Andreon et al. (2009, 2011).

Figure 6 shows the red (left panels) and blue (right panels) radial number profiles (upper panels) and radial density profiles (lower panels) for all three clusters, after accounting for the background. The three clusters have similar blue and red radial profiles, showing that the three clusters have similar richnesses.

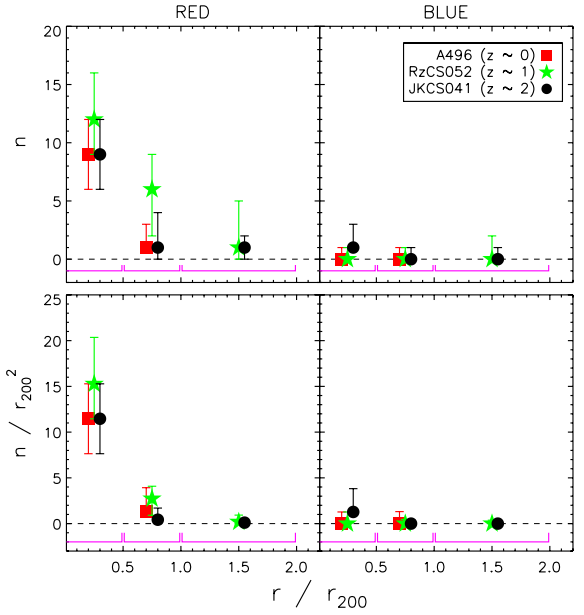


Fig. 6. Radial number profile (upper panels) and radial number density profile (lower panels) of red (left panels) and blue (right panels) member galaxies as a function of the cluster-centric distance, coded as indicated in the legend, after accounting for the background. The three radial ranges used are indicated by the magenta lines. Points indicate the maximum a posteriori, the error bars the shortest 68% interval. Points are slightly shifted horizontally for readability.

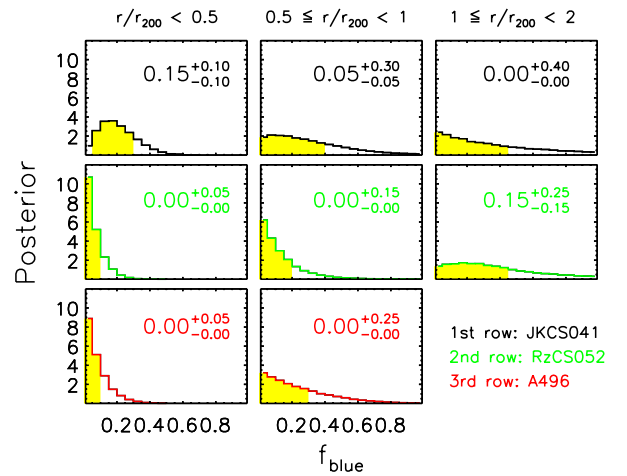


Fig. 7. Posterior probability distribution of the blue fraction for the three clusters (JKCS 041: upper row, RzCS 052: middle row, A496: lower row), in three radial ranges. The 68% shortest confidence intervals are shaded in yellow.

The right panel shows that all these three clusters have a negligible number of blue galaxies within $2 \times r_{200}$. Unfortunately, the low redshift of A496 prevents us from probing its outer regions.

Figure 7 shows the (posterior) probability distribution of the blue fractions of the three clusters in the three radial regions (two for A496) and summarises their properties (point estimates and 68% shortest interval). We emphasize that our f_{blue} computation requires the use of the full probability distributions for intervening quantities, n_{blue} and n_{red} , not just their point estimates and 68% uncertainties reported in Fig. 6.

Figure 8 shows the blue fraction profiles of the three clusters and our main result of this section: we observe the same

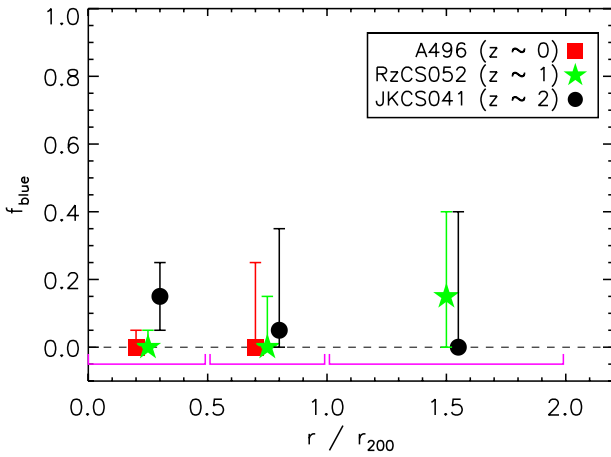


Fig. 8. Blue fraction as a function of the cluster-centric distance: JKCS 041 ($z \sim 2$, black dots), RzCS 052 ($z \sim 1$, green stars), and A496 ($z \sim 0$, red squares). Points indicate the maximum a posteriori, the error bars the shortest 68% interval. The three radial ranges used are indicated by the magenta lines. Abscissae are slightly shifted for readability.

(negligible) amount of blue galaxies more massive than $1.34 \times 10^{11} M_{\odot}$ all the way up to $z \sim 2.2$ in all radial bins. The values of f_{blue} are all less than 1.4σ away for all the three clusters in all the radial bins.

To quantify the sensitivity of our data to an evolving f_{blue} , we focus on the innermost bin ($r/r_{200} \leq 0.5$) of the two clusters at the redshift ends, A496 and JKCS 041, to maximize the redshift leverage. By looking at the posterior of $\Delta f_{\text{blue}} = f_{\text{blue}}^{\text{JKCS041}} - f_{\text{blue}}^{\text{A496}}$, we measure $\Delta f_{\text{blue}} \leq 0.36$ (resp. $\Delta f_{\text{blue}} \leq 0.18$) with 95% (resp. 68%) probability. Hence, the rate at which the blue fraction changes, $\Delta f_{\text{blue}}/\Delta z$, is less than 0.16 (resp. 0.08) per unit redshift at 95% (resp. 68%) probability. By a way of comparison, Butcher & Oemler (1984) found a slope of 0.5 for a roughly similar radial aperture, but for a sample that included galaxies with smaller masses. Although our error bars at $z \sim 2.2$ are large, the redshift leverage of this work allows us to tightly constrain the evolution of f_{blue} .

4.3. Robustness of the result on assumption

We test the sensitivity of our results to our assumptions: a) we change the redshift of JKCS 041 by ± 0.1 ; b) in place of the selection given in Eq. (1), we instead retain galaxies with at least a 30% probability (following Tran et al. 2010) of being in the $1.5 < z < 2.1$ range, i.e.

$$\int_{1.5}^{2.1} p(z) dz \geq 0.3; \quad (2)$$

and thirdly c) we use the $z' - J$ (rest-frame $\sim 2500\text{--}3000 \text{ \AA} - u^*$) instead of the $J - K_s$ colour index to identify red and blue galaxies. In these three cases, none of our measurements (both fractions and radial profiles) change, not even by 1σ . If instead of a mass-selected sample, we use a luminosity-selected sample brighter than an evolved $M_V = -20.8$ mag for all three clusters, then we derive consistent radial profiles for the three clusters, i.e. we continue to find no Butcher-Oemler effect.

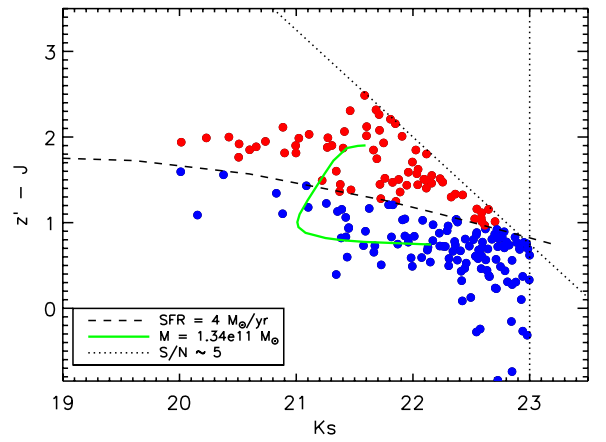


Fig. 9. Colour–magnitude diagram for galaxies along JKCS 041 line of sight (i.e. JKCS 041 and residual background galaxies) within $2 \times r_{200}$. The black dotted lines represent the $S/N = 5$ locii. The green solid line represents the locus of constant mass $M = 1.34 \times 10^{11} M_{\odot}$. The black dashed line indicates the locus of a constant SFR of $4 M_{\odot} \text{ yr}^{-1}$, distinguishing quiescent and star-forming galaxies.

5. Star formation activity

We now classify galaxies as either star-forming or quiescent, based on the slope of their UV continuum, specifically according to whether they are either bluer or redder in the $z' - J$ ($\sim L_{2800}/L_{3700}$) vs. K_s diagram than a CB07 model with solar metallicity, $z_{\text{form}} = 5$, and an exponential declining star formation history that has a star formation rate (SFR) equal to $4 M_{\odot} \text{ yr}^{-1}$ at $z = 1.8$. This SFR value is chosen according to the analysis of Kriek et al. (2009), who studied a $z \sim 2$ spectrum of a quiescent galaxy and found a maximum SFR of $4 M_{\odot} \text{ yr}^{-1}$ (for a Chabrier IMF). We underline that there is presently no reference SFR value at $z \sim 2$ used to classify a galaxy as quiescent: we chose the value of Kriek et al. (2009), because it relies on a spectroscopic measurement, though only on one object. Other works, such as Quadri et al. (2012), use a different criterion. In addition to our $M \geq 1.34 \times 10^{11} M_{\odot}$ mass-selected sample, we consider a sample of less massive galaxies, selected based on the data S/N . The latter choice has the advantage of enlarging the mass range, but the disadvantage of making it difficult, not to say impossible, to compare results derived from data of different depths or for clusters at different redshift. Figure 9 shows the data and the various relevant locii.

Using the same Bayesian methods used in Sect. 4 for red and blue galaxies, we compute the radial profile of quiescent and star-forming galaxies, as well as the radial profile of the star-forming fraction, shown in Fig. 10. This figure shows that there is a consistent and systematic increase in the fraction of star-forming galaxies with cluster-centric distance for both the sample with $M \geq 1.34 \times 10^{11} M_{\odot}$ (left panels) and the sample of less massive galaxies (right panels). This is the main result of this section.

Figure 11 shows that the local density, based on the distance of the seventh nearest neighbour, goes as a function of cluster-centric distance: it decreases with r/r_{200} until $r/r_{200} \sim 1$, after which its trend cannot be estimated because of uncertainties. We note that the cluster center is defined by the X-ray barycenter, not by the peak of the local density itself and thus the peak at low radii is not due to a selection effect. Since density and cluster-centric distance run hand in hand, at $z \sim 2.2$, the fraction of

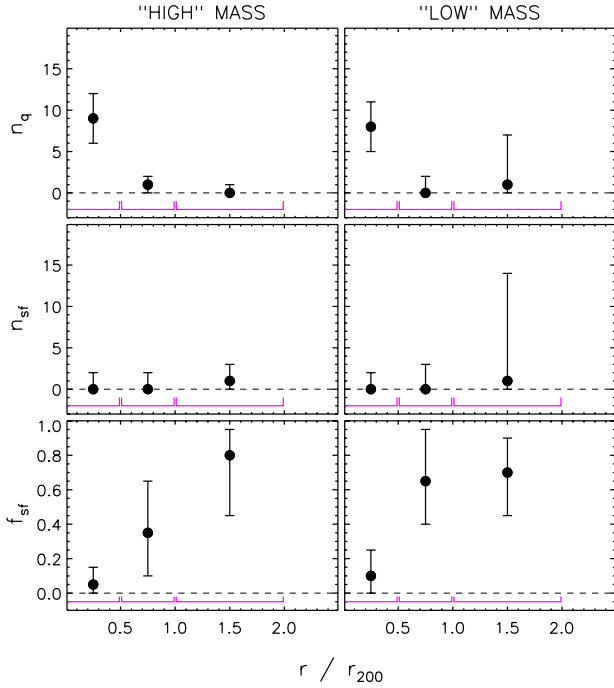


Fig. 10. JKCS 041 radial profiles of cluster quiescent n_q (upper row) and star-forming n_{sf} (middle row) galaxies, and the cluster star-forming fraction f_{sf} (lower row) for the high mass subsample (left column) and the less massive subsample (right column). The three radial ranges used are indicated by the magenta lines.

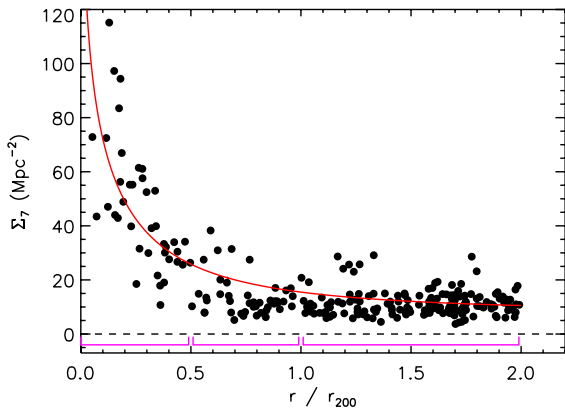


Fig. 11. Local density, estimated from the distance of the seventh nearest neighbor vs. JKCS 041 cluster-centric distance: for this figure only, galaxies are selected solely with a photometric redshift criterion (Eq. (1)) and $K_s \leq 23$ mag. The red line shows the best-fit model of a theoretical Navarro et al. (1996) profile plus a constant to take into account the background. The three radial ranges used for estimating f_{blue} and f_{sf} are indicated by the magenta lines.

star-forming galaxies decreases with density. For illustrative purposes, we plot in Fig. 12 the JKCS 041 star-forming fraction f_{sf} vs. background-subtracted density Σ_7 .

We emphasize that while the high-mass sample is complete (in mass), the sample of lower mass galaxies has a completeness that depends on whether the galaxy is quiescent or star-forming. This prevents any quantitative comparison of the star-forming fraction values between the two samples, because, for example, a larger fraction of star-forming galaxies among less massive galaxies may be genuine or just a selection effect, caused by the mass-incompleteness of low-mass quiescent galaxies, as already mentioned. On the other hand, this selection effect is

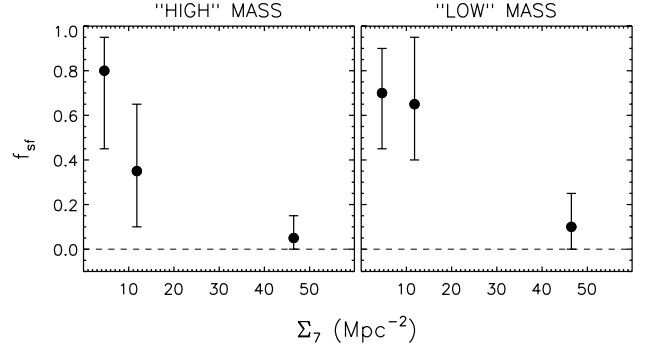


Fig. 12. JKCS 041 star-forming fraction f_{sf} vs. density Σ_7 for the high-mass subsample (left column) and the less massive subsample (right column). The plotted values for Σ_7 are the mean values of the best-fit profile in Fig. 11 (red line) for each radial range, after background subtraction.

independent of the cluster-centric distance and thus does not affect our conclusion about the increase in the fraction of star-forming galaxies with cluster-centric distance.

We test the sensitivity of our results to our assumptions: a) we change the redshift of JKCS 041 by ± 0.1 ; b) we use Eq. (2) for photometric redshift pre-selection; c) we multiply/divide by two the SFR threshold value used to define quiescent/star-forming galaxies; d) we classify galaxies as either star-forming or quiescent based on their position in the $U-V$ vs. $V-J$ plane, in a similar way to Williams et al. (2009) and Quadri et al. (2012). We emphasize that in case d) the classification is almost identical to the one of Fig. 9, but that our rest-frame J photometry was derived by extrapolating the available multicolour photometry. Our result does not change after applying case a). For cases b), c), and d), we observe a radial profile increase with cluster-centric distance, i.e. that the star formation-density relation is already in place at $z \sim 2.2$. We stress that in all cases, the fraction of massive star-forming galaxies within $r_{200}/2$ is very low ($\leq 15\%$, 1σ error bars included).

6. Discussion and conclusions

We have taken advantage of the availability of CFHTLS ($u^*g'r'i'z'$ bands) and WIRDS (JHK_s bands) images to study the JKCS 041 cluster. Using two lower redshift clusters of similar mass (RzCS 052 at $z = 1.016$ and A496 at $z = 0.032$) as a comparison sample, we have studied the evolution with redshift of cluster galaxies properties. Our results are:

1. By using photometric redshifts, we have confirmed that JKCS 041 is a high redshift cluster, in agreement with Andreon & Huertas-Company (2011). Our photometric redshift estimate is $z_{\text{phot}} = 2.00^{+0.02}_{-0.03}$ (1σ errors), after a systematic correction of $\delta z = 0.2$ extrapolated from $z \lesssim 1.5$.
2. Working on a mass-limited sample ($M \geq 1.34 \times 10^{11} M_{\odot}$) and taking into account the star aging with decreasing redshift, we have measured the same (negligible) fraction of blue galaxies all the way to $z \sim 2.2$ in all radial bins within $2 \times r/r_{200}$: we thus do not observe any evidence of any Butcher-Oemler effect between $z \sim 2.2$ and $z \sim 0$. For our definition of blue galaxy, very few galaxies more massive than $M = 1.34 \times 10^{11} M_{\odot}$ are found to be blue, for all redshifts and radii. Although error bars are large, the redshift leverage of this work is at least twice as large as in any previous work, allowing us to reject with confidence a change greater than $\Delta f_{\text{blue}}/\Delta z = 0.16$ at the cluster center.

3. The cluster JKCS 041 shows a consistent and systematic increase in the fraction of star-forming galaxies with cluster-centric distance for both the $M \geq 1.34 \times 10^{11} M_{\odot}$ sample and a sample of less massive galaxies. In particular, very few (less than 15%) star-forming galaxies are found within $r_{200}/2$ among high mass galaxies.
4. The local galaxy density decreases with increasing cluster-centric distance for $r \leq r_{200}$, and thus our statements above may be rephrased in terms of local density.

Andreon et al. (2008b) led a very similar analysis of the Butcher-Oemler effect for RzCS 052 and A496, the only difference being that a lower mass cut is used ($M \geq 4 \times 10^{10} M_{\odot}$). Interestingly, they found an evolution in the fraction of blue galaxies between $z \sim 1$ and $z \sim 0$, which we have not found. Gathering their and our results together, we have found that our results are consistent with a *downsizing*-like scenario (e.g. Cowie et al. 1996; Treu et al. 2005; Iovino et al. 2010; Peng et al. 2010), where the properties of the most massive galaxies are established in the very early Universe ($z \gg 1$), while less massive galaxies continue to evolve at redshifts $0 < z < 1$.

Our observations of JKCS 041 show that most bright core cluster galaxies are red and passive at $z \sim 2.2$, an observation that models still have difficulties in reproducing (e.g. Menci et al. 2008; Romeo et al. 2008).

Our detection of a star formation-density relation in JKCS 041 is in agreement with the results of Chuter et al. (2011) and Quadri et al. (2012) at $z \lesssim 1.8$ and those for the XMMU J2235-2557 cluster at $z = 1.39$ (Lidman et al. 2008; Rosati et al. 2009; Strazzullo et al. 2010; Bauer et al. 2011) and in disagreement with the studies of the XMMXCS J2215.9-1738 cluster at $z = 1.46$ (Hayashi et al. 2010; Hilton et al. 2010).

This variety of results may be either a manifestation of a spread in the star formation-density relations at high redshift – perhaps related to the cluster dynamical status, or just the result of unidentified systematic errors. Enlarging the sample used for the Butcher-Oemler effect – and particularly selecting likely low redshift descendants of JKCS 041 – and deepening the analysis of the star formation activity in JKCS 041 is necessary to strengthen our results, and will be addressed in future work. However, the cluster JKCS 041 is a uniquely suitable target for galaxy evolutionary studies, even if it presently has only photometric redshift data, because it is so far the only $z \gtrsim 1.5$ cluster with measured intra-cluster medium properties – hence r_{200} – and a sizable red population. More clusters with robust estimates of their mass are needed to consolidate the link, put forth by JKCS 041, between star formation and environment at high redshift.

Acknowledgements. We acknowledge financial contribution from the agreement ASI-INAF I/009/10/0 and from Osservatorio Astronomico di Brera. Based on observations obtained with MegaPrime/MegaCam (full acknowledgement is at <http://www.cfht.hawaii.edu/Science/CFHLS/cfhtlspublitext.html>) and WIRCAM at CFHT (<http://ftp.cfht.hawaii.edu/Instruments/Imaging/WIRCam/WIRCamAcknowledgment.html>).

References

Abell, G. O. 1958, *ApJS*, 3, 211
 Andreon, S. 2001, *ApJ*, 547, 623
 Andreon, S. 2006, in *The Fabulous Destiny of Galaxies: Bridging Past and Present*, ed. V. Le Brun, A. Mazure, S. Arnouts, & D. Burgarella, 463
 Andreon, S. 2011, *A&A*, 529, L5
 Andreon, S., & Ettori, S. 1999, *ApJ*, 516, 647

Andreon, S., & Huertas-Company, M. 2011, *A&A*, 526, A11
 Andreon, S., Lobo, C., & Iovino, A. 2004, *MNRAS*, 349, 889
 Andreon, S., Quintana, H., Tajer, M., Galaz, G., & Surdej, J. 2006, *MNRAS*, 365, 915
 Andreon, S., de Propris, R., Puddu, E., Giordano, L., & Quintana, H. 2008a, *MNRAS*, 383, 102
 Andreon, S., Puddu, E., de Propris, R., & Cuillandre, J. 2008b, *MNRAS*, 385, 979
 Andreon, S., Maughan, B., Trinchieri, G., & Kurk, J. 2009, *A&A*, 507, 147
 Andreon, S., Trinchieri, G., & Pizzolato, F. 2011, *MNRAS*, 73
 Barro, G., Pérez-González, P. G., Gallego, J., et al. 2011, *ApJS*, 193, 30
 Bauer, A. E., Grützbauch, R., Jørgensen, I., Varela, J., & Bergmann, M. 2011, *MNRAS*, 411, 2009
 Bertin, E., & Arnouts, S. 1996, *A&AS*, 117, 393
 Bielby, R., Hudelot, P., McCracken, H. J., Ilbert, O., et al. 2011, *A&A*, submitted [arXiv:1111.6997]
 Braglia, F. G., Pierini, D., Biviano, A., & Böhringer, H. 2009, *A&A*, 500, 947
 Brammer, G. B., van Dokkum, P. G., & Coppi, P. 2008, *ApJ*, 686, 1503
 Brodwin, M., Brown, M. J. I., Ashby, M. L. N., et al. 2006, *ApJ*, 651, 791
 Bruzual, G., & Charlot, S. 2003, *MNRAS*, 344, 1000
 Butcher, H., & Oemler, Jr., A. 1984, *ApJ*, 285, 426
 Casertano, S., de Mello, D., Dickinson, M., et al. 2000, *AJ*, 120, 2747
 Chabrier, G. 2003, *PASP*, 115, 763
 Chuter, R. W., Almaini, O., Hartley, W. G., et al. 2011, *MNRAS*, 413, 1678
 Cooper, M. C., Newman, J. A., Weiner, B. J., et al. 2008, *MNRAS*, 383, 1058
 Coupon, J., Ilbert, O., Kilbinger, M., et al. 2009, *A&A*, 500, 981
 Cowie, L. L., Gardner, J. P., Hu, E. M., et al. 1994, *ApJ*, 434, 114
 Cowie, L. L., Songaila, A., Hu, E. M., & Cohen, J. G. 1996, *AJ*, 112, 839
 De Propris, R., Stanford, S. A., Eisenhardt, P. R., & Dickinson, M. 2003, *ApJ*, 598, 20
 De Propris, R., Colless, M., Peacock, J. A., et al. 2004, *MNRAS*, 351, 125
 Elbaz, D., Daddi, E., Le Borgne, D., et al. 2007, *A&A*, 468, 33
 Finlator, K., Ivezić, Ž., Fan, X., et al. 2000, *AJ*, 120, 2615
 Goto, T. 2005, *MNRAS*, 356, L6
 Haines, C. P., Smith, G. P., Egami, E., et al. 2009, *ApJ*, 704, 126
 Hayashi, M., Kodama, T., Koyama, Y., et al. 2010, *MNRAS*, 402, 1980
 Hilton, M., Lloyd-Davies, E., Stanford, S. A., et al. 2010, *ApJ*, 718, 133
 Hogg, D. W., Blanton, M. R., Eisenstein, D. J., et al. 2003, *ApJ*, 585, L5
 Ilbert, O., Arnouts, S., McCracken, H. J., et al. 2006, *A&A*, 457, 841
 Ilbert, O., Capak, P., Salvato, M., et al. 2009, *ApJ*, 690, 1236
 Iovino, A., Cucciati, O., Scodreggio, M., et al. 2010, *A&A*, 509, A40
 Jee, M. J., Rosati, P., Ford, H. C., et al. 2009, *ApJ*, 704, 672
 Kauffmann, G., White, S. D. M., Heckman, T. M., et al. 2004, *MNRAS*, 353, 713
 Koyama, Y., Kodama, T., Shimasaku, K., et al. 2010, *MNRAS*, 403, 1611
 Kriek, M., van Dokkum, P. G., Labbé, I., et al. 2009, *ApJ*, 700, 221
 Lawrence, A., Warren, S. J., Almaini, O., et al. 2007, *MNRAS*, 379, 1599
 Le Fèvre, O., Vettolani, G., Garilli, B., et al. 2005, *A&A*, 439, 845
 Lidman, C., Rosati, P., Tanaka, M., et al. 2008, *A&A*, 489, 981
 Loh, Y.-S., Ellingson, E., Yee, H. K. C., et al. 2008, *ApJ*, 680, 214
 Longhetti, M., & Saracco, P. 2009, *MNRAS*, 394, 774
 Menci, N., Rosati, P., Gobat, R., et al. 2008, *ApJ*, 685, 863
 Navarro, J. F., Frenk, C. S., & White, S. D. M. 1996, *ApJ*, 462, 563
 Oemler, Jr., A. 1974, *ApJ*, 194, 1
 Papovich, S., Momcheva, I., Willmer, C. N. A., et al. 2010, *ApJ*, 716, 1503
 Patel, S. G., Holden, B. P., Kelson, D. D., Illingworth, G. D., & Franx, M. 2009, *ApJ*, 705, L67
 Patel, S. G., Kelson, D. D., Holden, B. P., Franx, M., & Illingworth, G. D. 2011, *ApJ*, 735, 53
 Peng, Y.-J., Lilly, S. J., Kovač, K., et al. 2010, *ApJ*, 721, 193
 Quadri, R. F., Williams, R. J., Franx, M., & Hildebrandt, H. 2012, *ApJ*, 744, 88
 Rines, K., Geller, M. J., Kurtz, M. J., & Diaferio, A. 2005, *AJ*, 130, 1482
 Romeo, A. D., Napolitano, N. R., Covone, G., et al. 2008, *MNRAS*, 389, 13
 Rosati, P., Tozzi, P., Gobat, R., et al. 2009, *A&A*, 508, 583
 Schlegel, D. J., Finkbeiner, D. P., & Davis, M. 1998, *ApJ*, 500, 525
 Sobral, D., Best, P. N., Smail, I., et al. 2011, *MNRAS*, 411, 675
 Stanford, S. A., Romer, A. K., Sabirli, K., et al. 2006, *ApJ*, 646, L13
 Strazzullo, V., Rosati, P., Pannella, M., et al. 2010, *A&A*, 524, A17
 Struble, M. F., & Rood, H. J. 1999, *ApJS*, 125, 35
 Tanaka, M., Lidman, C., Bower, R. G., et al. 2009, *A&A*, 507, 671
 Tanaka, M., Finoguenov, A., & Ueda, Y. 2010, *ApJ*, 716, L152
 Tran, K., Papovich, C., Saintonge, A., et al. 2010, *ApJ*, 719, L126
 Treu, T., Ellis, R. S., Kneib, J., et al. 2003, *ApJ*, 591, 53
 Treu, T., Ellis, R. S., Liao, T. X., & van Dokkum, P. G. 2005, *ApJ*, 622, L5
 Williams, R. J., Quadri, R. F., Franx, M., van Dokkum, P., & Labbé, I. 2009, *ApJ*, 691, 1879